Available online at www.sciencedirect.com
SCIENCE DIRECT®
Comput. Methods Appl. Mech. Engrg. 194 (2005) 367–381
Computer methods in applied mechanics and engineering
www.elsevier.com/locate/cma

Wave interpolation finite elements for Helmholtz problems with jumps in the wave speed

O. Laghrouche [a,*], P. Bettess [b], E. Perrey-Debain [c], J. Trevelyan [b]

[a] School of the Built Environment, Heriot-Watt University, Edinburgh EH14 4AS, UK
[b] School of Engineering, University of Durham, Durham DH1 3LE, UK
[c] Department of Mathematics, University of Manchester, Manchester M13 9PL, UK

Received 17 October 2003; received in revised form 2 December 2003; accepted 2 December 2003

Abstract

Finite elements for short wave scattering problems have recently been developed by various authors. These have almost exclusively dealt with the Helmholtz equation. The elements have been very successful, in terms of drastic reductions of the number of degrees of freedom in the numerical model. However, most of them are not directly applicable to problems in which the wave speed is not constant, but varies with position. Many important wave problems fall into this latter category. This is because short waves are often present in materials whose properties vary in space. The present paper demonstrates how the method may be extended so as to deal with problems in which the wave speed is piecewise constant, in various regions of the problem domain. Lagrange multipliers are used to enforce the necessary conditions of compatibility between the different regions. The paper gives numerical results, for problems for which the analytical solution is known. This shows how these methods may be extended, in a relatively simple fashion, to solve a much larger class of wave problems, of great practical interest.

Keywords: Helmholtz equation; Finite elements; Plane wave basis; Lagrange multipliers; Wave scattering

1. Introduction

This paper is concerned with the development of the plane wave basis finite element to deal with problems in which the wave speeds vary in space. In particular it is oriented towards the problem of the refraction and scattering of waves where they are step changes in the wave speed. There are many cases of practical importance where this may occur, including:

* Corresponding author.

0045-7825/$ - see front matter
doi:10.1016/j.cma.2003.12.074

- Electromagnetic waves propagating from air into a material with different electromagnetic constants, for example parts of a ship, aeroplane or road vehicle.
- Surface waves on water propagating from a zone with one constant depth, to a zone with another constant depth.
- Elastic waves in rocks, used in hydrocarbon prospecting, traversing from rocks of a certain density and stiffness into rocks of a different density and stiffness.
- Ultrasound waves propagating through human tissue of varying properties.
- Propagation of noise through the air, especially where there are temperature changes, and through vehicles.

The classical finite element method is severely constrained in dealing with short wave scattering problems because typically about 10 nodes per wavelength are needed for results of engineering accuracy. More precise error estimates which take into account the *pollution errors* and the order of the element polynomials are available [1–4]. This problem is well known and will not be dwelt on at length here. Because of this difficulty, in recent years a great deal of attention has been applied to methods which incorporate a knowledge of the waves in the formulation, and so escape the above limitation. This limitation is true for both domain based (finite element, finite differences and finite volume) and boundary based methods (boundary integrals).

So much activity has been taking place in these fields that a comprehensive survey is not possible. The reader is directed to Refs. [5,6] for background information and further references. The common feature of most of the new approaches is that analytical solutions to the Helmholtz equation are used to enrich the solution space. These are usually in the form of plane waves, but may also be in terms of cylindrical or spherical waves. These methods have been very effective. The plane wave basis finite elements offer an easy way to include analytical information about the problem to be solved. A number of authors have developed special finite and boundary elements for short wave scattering problems governed by the homogeneous Helmholtz equation, see for example [7–15]. Different aspects of the method, including integration and conditioning, have been studied. Note that Farhat et al. have added plane wave solutions to the conventional finite element polynomials and then enforced continuity through the use of Lagrange Multipliers [14,15]. Plane wave basis finite elements and boundary elements were also developed to deal with three dimensional wave scattering problems [16,17]. In a recent work, Astley and Gammalo [18], used the plane wave enrichment to model wave propagation on inhomogeneous mean flows in one and two dimensions where the wavenumber is a function of the Mach number.

The problem in dealing with discontinuities of material properties is that they cause changes in wave speed and wave number. The analytical solutions for the homogeneous Helmholtz equation are no longer valid when the equation becomes inhomogeneous, due to change in wave speed. Several authors have developed methods which are valid where there is a jump in the material properties between zones of the problem. The Ultra Weak formulation of Cessenat and Després [19] has been extended by Huttunen et al. to both scalar waves and elastic waves [20,21]. They have presented solutions for waves propagating through materials of different properties. In the latter case, they were developing a simplified model of waves propagating through the human skull, as part of a therapeutic system. Bettess [22] and Ortiz [23] have also considered problems in which the wave speed varies continuously, rather than in jumps between regions. As described above other authors have developed similar methods to that described here. However, so far as we are aware, there has been no systematic study of the accuracies obtained while modelling interfaces between zones of different wave speeds. The main aims of this paper are to arrive at the most effective way of enforcing compatibility between zones by the use of Lagrange Multipliers, to study the accuracy of the interface conditions, and to establish whether all the evanescent interface conditions are correctly modelled, for a range of material properties. The accuracy of this approach is investigated by comparisons with analytical solutions, including pathological cases.

2. Helmholtz equation in piecewise constant wave speed subdomains

In this work, we deal with multiple subdomains problems with discontinuities at the boundaries and constant wave speed in each of them. It is sufficient to consider the two subdomains problem showed in Fig. 1. We begin by considering the solution of the Helmholtz equation expressed in terms of the scalar potential Φ_1 in the subdomain Ω_1 bounded by $\Gamma_1 \cup \Gamma_{\text{int}}$.

$$(\nabla^2 + k_1^2)\Phi_1 = 0 \quad \text{in } \Omega_1, \tag{1}$$

where ∇^2 denotes the Laplacian operator and k_1 is the wave number in the subdomain Ω_1. The time variable is removed by considering a harmonic steady state. Robin boundary conditions are specified on the boundary Γ_1. These are

$$\nabla\Phi_1 \cdot \boldsymbol{n}_1 + \mathrm{i}k_1\Phi_1 = g_1 \quad \text{on } \Gamma_1, \tag{2}$$

where g_1 is the boundary condition, ∇ is the gradient vector operator, $\boldsymbol{n}_1$ is the outward normal to the line boundary $\Gamma_1 \cup \Gamma_{\text{int}}$ and i is the complex imaginary such that $\mathrm{i}^2 = -1$.

3. Weighted residual scheme

The differential equation (1) is multiplied by an arbitrary weight function W_1 and then integrated by parts to give the weak form

$$B(W_1, \Phi_1) = L(W_1), \tag{3}$$

where B stands for the bilinear form

$$B(W_1, \Phi_1) = \int_{\Omega_1} (\nabla W_1 \cdot \nabla\Phi_1 - k_1^2 W_1 \Phi_1)\,\mathrm{d}\Omega + \mathrm{i}k_1 \int_{\Gamma_1} W_1 \Phi_1\,\mathrm{d}\Gamma - \int_{\Gamma_{\text{int}}} W_1 \nabla\Phi_1 \cdot \boldsymbol{n}_1\,\mathrm{d}\Gamma \tag{4}$$

and

$$L(W_1) = \int_{\Gamma_1} W_1 g_1\,\mathrm{d}\Gamma. \tag{5}$$

Following the same procedure, we obtain for the subdomain Ω_2 bounded by $\Gamma_2 \cup \Gamma_{\text{int}}$ the weak form

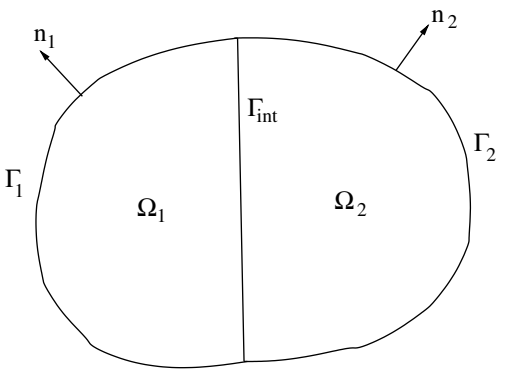

Fig. 1. Studied example.

$$B(W_2, \Phi_2) = L(W_2), \tag{6}$$

where all functions and parameters are defined in a similar way as for the weak form (3) replacing the subscript 1 by 2.

4. Plane wave basis finite elements

The two subdomains are divided into n-noded finite elements. In each finite element, the potential is first written as a polynomial interpolation of the nodal values of the potential. Then each nodal potential is approximated by a discrete sum of plane waves propagating in different directions in the plane. The unknowns are no longer the nodal values of the potential but are now the amplitudes attached to each node with respect to each direction of the chosen plane waves. In our case, a number m_j of plane waves are used in the approximating system at the node j which reads as follow

$$\Phi_1 = \sum_{j=1}^{n} \sum_{l=1}^{m_j} N_j \exp(\mathrm{i}k_1 \boldsymbol{\xi}_l \cdot \boldsymbol{r}) A_{jl}^{(1)}, \tag{7}$$

$$\Phi_2 = \sum_{j=1}^{n} \sum_{l=1}^{m_j} N_j \exp(\mathrm{i}k_2 \boldsymbol{\xi}_l \cdot \boldsymbol{r}) A_{jl}^{(2)}. \tag{8}$$

The number of the approximating plane waves may vary from one node to another. Their chosen directions could be evenly spaced or clustered around directions of preference. Though there is no restriction concerning the directions $\boldsymbol{\xi}_l$, these are taken to be evenly distributed on the unit circle,

$$\boldsymbol{\xi}_l = (\cos\theta_l, \sin\theta_l) \quad \text{with } \theta_l = 2\pi l/m_j. \tag{9}$$

where r and θ are the polar coordinates. For notational convenience, let us put the new shape function $P_{jl}^{(1)}$ and $P_{jl}^{(2)}$ as the product of the polynomial shape function N_j and the plane waves $\exp(\mathrm{i}k_1 \boldsymbol{\xi}_l \cdot \boldsymbol{r})$ and $\exp(\mathrm{i}k_2 \boldsymbol{\xi}_l \cdot \boldsymbol{r})$, respectively. In a matricial form, the potentials of expressions (7) and (8) would be written as $\Phi_1 = \boldsymbol{P}_1 \boldsymbol{A}_1$ and $\Phi_2 = \boldsymbol{P}_2 \boldsymbol{A}_2$ where $\boldsymbol{A}_1$ and $\boldsymbol{A}_2$ are the vectors of the unknowns amplitudes. The vectors $\boldsymbol{P}_1$ and $\boldsymbol{P}_2$ contain the oscillatory shape functions which are products of polynomials and planar waves.

5. Continuity between subdomains

At the interface boundary Γ_{int} continuity of potential and flux equilibrium condition must be satisfied (Fig. 2)

$$\Phi_1 = \Phi_2 \tag{10}$$

and

$$\frac{1}{k_1^2} \nabla \Phi_1 \cdot \boldsymbol{n}_1 + \frac{1}{k_2^2} \nabla \Phi_2 \cdot \boldsymbol{n}_2 = 0. \tag{11}$$

For this, we consider a Lagrangian multiplier method such that

$$\lambda = \frac{1}{k_1^2} \nabla \Phi_1 \cdot \boldsymbol{n}_1 = -\frac{1}{k_2^2} \nabla \Phi_2 \cdot \boldsymbol{n}_2 \tag{12}$$

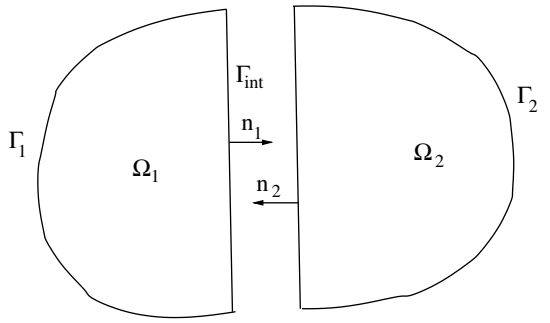

Fig. 2. Two subdomains with a common interface boundary.

The two bilinear forms of (3) and (6) are then written as

$$B(W_1,\Phi_1)=\int_{\Omega_1}(\nabla W_1\cdot\nabla\Phi_1-k_1^2W_1\Phi_1)\,\mathrm{d}\Omega+\mathrm{i}k_1\int_{\Gamma_1}W_1\Phi_1\,\mathrm{d}\Gamma-k_1^2\int_{\Gamma_{\mathrm{int}}}W_1\lambda\,\mathrm{d}\Gamma, \tag{13}$$

$$B(W_2,\Phi_2)=\int_{\Omega_2}(\nabla W_2\cdot\nabla\Phi_2-k_2^2W_2\Phi_2)\,\mathrm{d}\Omega+\mathrm{i}k_2\int_{\Gamma_2}W_2\Phi_2\,\mathrm{d}\Gamma+k_2^2\int_{\Gamma_{\mathrm{int}}}W_2\lambda\,\mathrm{d}\Gamma. \tag{14}$$

In the discontinuous enrichment method developed by Farhat et al. [15], the Lagrange multipliers are approximated by oscillatory functions with the wave number of the Helmholtz problem (Fig. 3). However, in this case, the edge element corresponding to the Lagrange multipliers is on the boundary between two elements with different wave numbers. In this study, the variable λ is approximated using the same approach for the approximation of the potentials Φ_1 and Φ_2. A priori, using the lower wave number in the interpolation of λ may not capture the oscillatory behaviour on the edge of the element with the higher wave number. The interpolation for the unknown λ is given by

$$\lambda=\sum_{j=1}^{p}\sum_{l=1}^{m_j}N_j\exp(\mathrm{i}k\boldsymbol{\xi}_l\cdot\boldsymbol{r})\lambda_{jl}, \tag{15}$$

where $k=\max(k_1,k_2)$ and λ_{jl} are the Lagrange multipliers at node j with respect to direction $\boldsymbol{\xi}_l$. For convenience, let us put $Q_{jl}=N_j\exp(\mathrm{i}k\boldsymbol{\xi}_l\cdot\boldsymbol{r})$ and then $\lambda=\boldsymbol{Q}\boldsymbol{\lambda}$. A Galerkin scheme is used so that the weighting functions are chosen to be the same as the interpolating oscillatory functions. The two sets of Galerkin equations of expressions (13) and (14) may be written in a matricial form

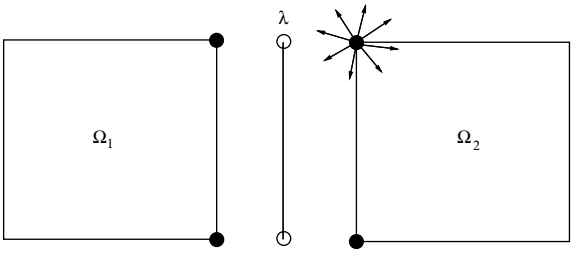

Fig. 3. Duplication of nodes at the interface Γ_{int} and introduction of Lagrange multipliers.

$$\begin{cases} H_1 \boldsymbol{A}_1 - C_1 \boldsymbol{\lambda} = \boldsymbol{f}_1, \\ H_2 \boldsymbol{A}_2 + C_2 \boldsymbol{\lambda} = \boldsymbol{f}_2, \end{cases} \tag{16}$$

where

$$H_1 = \int_{\Omega_1} (\nabla \boldsymbol{P}_1^{\mathrm{T}} \nabla \boldsymbol{P}_1 - k_1^2 \boldsymbol{P}_1^{\mathrm{T}} \boldsymbol{P}_1)\, \mathrm{d}\Omega + \mathrm{i}k_1 \int_{\Gamma_1} \boldsymbol{P}_1^{\mathrm{T}} \boldsymbol{P}_1\, \mathrm{d}\Gamma, \tag{17}$$

$$C_1 = k_1^2 \int_{\Gamma_{\mathrm{int}}} \boldsymbol{P}_1^{\mathrm{T}} \boldsymbol{Q}\, \mathrm{d}\Gamma, \tag{18}$$

and

$$\boldsymbol{f}_1 = \int_{\Gamma_1} \boldsymbol{P}_1^{\mathrm{T}} g_1\, \mathrm{d}\Gamma. \tag{19}$$

For the second set of equations in the system (16), the matrices are obtained in the same way by replacing subscript 1 by 2. At this stage, there are more unknowns than equations. Therefore, we add the continuity condition as

$$\int_{\Gamma_{\mathrm{int}}} \boldsymbol{Q}^{\mathrm{T}} [\Phi_2 - \Phi_1]\, \mathrm{d}\Gamma = 0 \tag{20}$$

Substituting the approximations for the fields, then writing compactly the above steps gives the following system to solve

$$\begin{bmatrix} H_1 & 0 & -C_1 \\ 0 & H_2 & C_2 \\ -C_1^{\mathrm{T}} & C_2^{\mathrm{T}} & 0 \end{bmatrix} \begin{Bmatrix} \boldsymbol{A}_1 \\ \boldsymbol{A}_2 \\ \boldsymbol{\lambda} \end{Bmatrix} = \begin{Bmatrix} \boldsymbol{f}_1 \\ \boldsymbol{f}_2 \\ 0 \end{Bmatrix}. \tag{21}$$

Note that the last diagonal block is formed by zero elements. During the solution process, adequate line and column permutations are performed to avoid singularity of the system. This could be achieved by an appropriate numbering of the mesh nodal points.

6. Straight depth discontinuity—oblique incidence

Consider a plane wave with a unit amplitude propagating on the surface of water (x, y) at an angle θ_I with the x axis as indicated on Fig. 4. The wave travels from shallow to deep water where the y axis is at the discontinuity. The depths, in the z direction, are h_1 for $x < 0$ and h_2 for $x > 0$. The incident wave $\phi_I = \exp(\mathrm{i}k_1 r \cos(\theta - \theta_I))$ is reflected at $x = 0$, $\phi_R = R \exp(\mathrm{i}k_1 r \cos[\theta - (\pi - \theta_I)])$ and transmitted to the deep side $\phi_{\mathrm{T}} = T \exp(\mathrm{i}k_1 r \cos(\theta - \theta_{\mathrm{T}}))$ where R and T are the reflected and transmission coefficients, respectively. They are obtained by matching the surface potential and the volume flux at the discontinuity. The angle θ_{T} of the transmitted wave is obtained using Snell's law. For a fixed frequency, the two wave numbers k_1 and k_2 are fixed by h_1 and h_2. The quadrant at the surface of water, $-5 \leqslant x, y \leqslant 5$, is meshed into 4-noded finite elements (Fig. 4). All dimensions are relative to a unit of length. A plane wave is incident at $\theta_I = 15^\circ$ and the wave numbers considered are $k_1 = 2\pi$ and $k_2 = \pi$. The exact solution is imposed on the boundary of the mesh through boundary conditions g_1 and g_2 given by expression (2), (for g_2, change subscript 1 by 2). A system of 18 plane waves with evenly spaced directions are attached to each node to approximate the potentials Φ_1 and Φ_2. Note that none of the angles θ_I, $\pi - \theta_I$ and θ_{T}, which is equal to 31.2°, is included in the directions of the approximating plane waves. The test functions and the trial functions are combina-

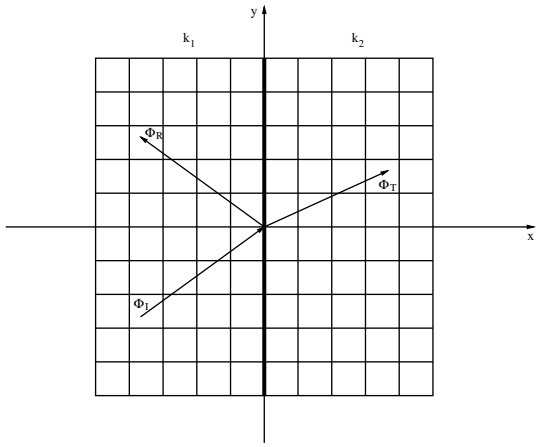

Fig. 4. Straight depth discontinuity with an oblique incidence.

tions of plane waves. This leads us to integrate oscillatory functions to obtain the element matrices of the system (21). Special integration rules were developed to integrate such forms in two dimensions [11,24,25]. In this paper, all integrals are evaluated using high order Gauss–Legendre schemes. Fig. 5 shows the real

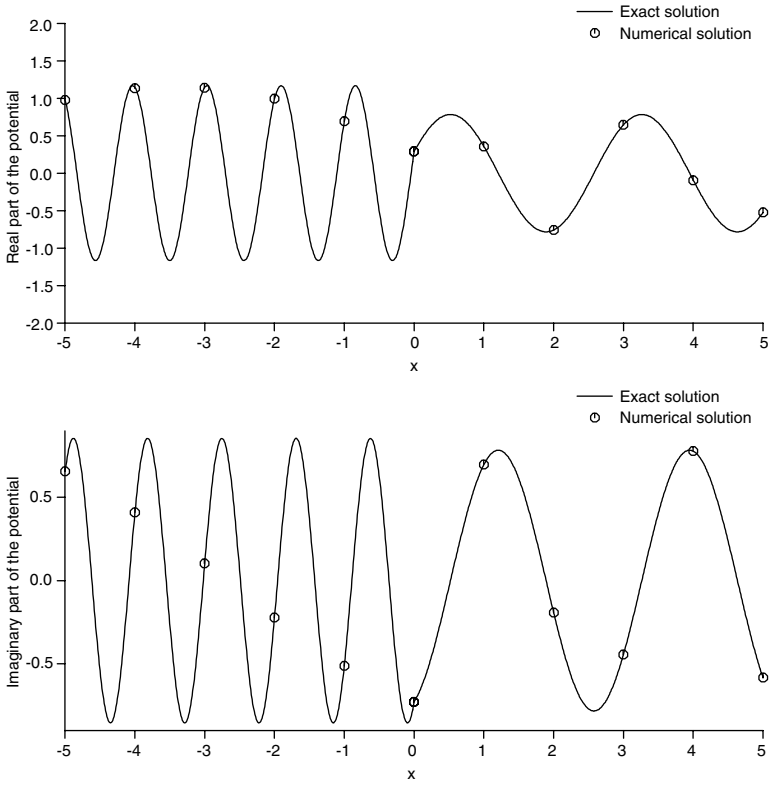

Fig. 5. Transmitted plane wave from shallow to deep water.

and imaginary parts of the potential along $y = 0$ for the analytical solution and the numerical results. It is clear from the figure that the wavelength in the shallow water is shorter than the one in the deep water. At the interface, ($x = 0$), the nodes are duplicated and therefore two numerical results are obtained, which are identical thanks to the continuity imposed by the Lagrange multipliers. If the angle of incidence θ_I reaches the critical value

$$(\theta_I)_c = \tan^{-1}\left(\frac{k_2}{\sqrt{k_1^2 - k_2^2}}\right) \tag{22}$$

the transmitted wave propagates along the discontinuity. When θ_I increases beyond $(\theta_I)_c$, the transmitted wave propagates along the y axis with amplitude decaying exponentially in the x direction. This is termed an *evanescent* wave. This is shown in Fig. 6. For the wavenumbers given above, the critical angle takes the value of 30°. The angle of incidence is chosen to be $\theta_I = 45°$ which will give an evanescent transmitted wave. The numerical results are in good agreement with the analytical answer. This shows the ability of the method to capture the described phenomenon. Despite the fact that the plane waves attached to each node correspond to real wave numbers, the method can still efficiently approximate wave problems with exponential decays.

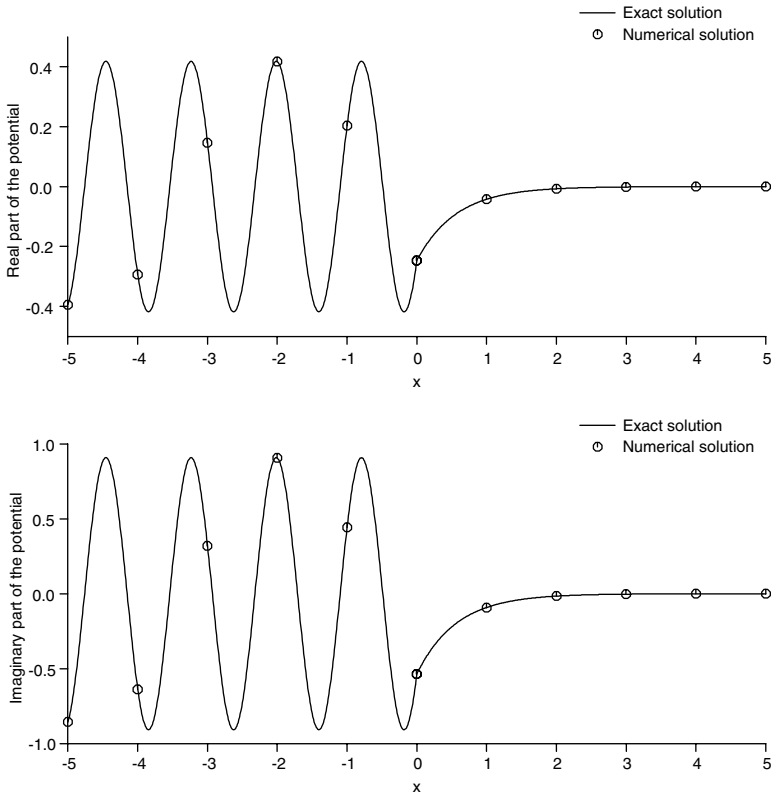

Fig. 6. Transmitted wave with exponential decay.

7. Plane wave scattering by a rigid cylinder

This example deals with the diffraction of a plane wave by a rigid circular cylinder, of radius r_1, which is assumed to be vertical and the plane wave is incident horizontally on the surface of water. Around the cylinder, the water is of depth h_1 up to a circular region of radius r_2. Then for $r \geqslant r_2$, the depth is h_2. On Fig. 7, the outer region is deeper than the one around the cylinder ($h_1 < h_2$). However, the theory remains the same if $h_1 > h_2$. The physical domain of this problem is infinite in extent. This means that it must be truncated at a finite distance from the scatterrer to enable a numerical simulation. The outer boundary deemed to represent infinity is then represented by the boundary Γ_2 situated at $r = r_3$ (Fig. 8).

7.1. Analytical solution

A solution to this problem has been developed in terms of Bessel function series. Note that three dimensional effects occurring due to the changes in depth have been ignored in these examples, since they are not relevant to the assessment of the method. The potentials in the regions Ω_1 and Ω_2 are given, respectively, by

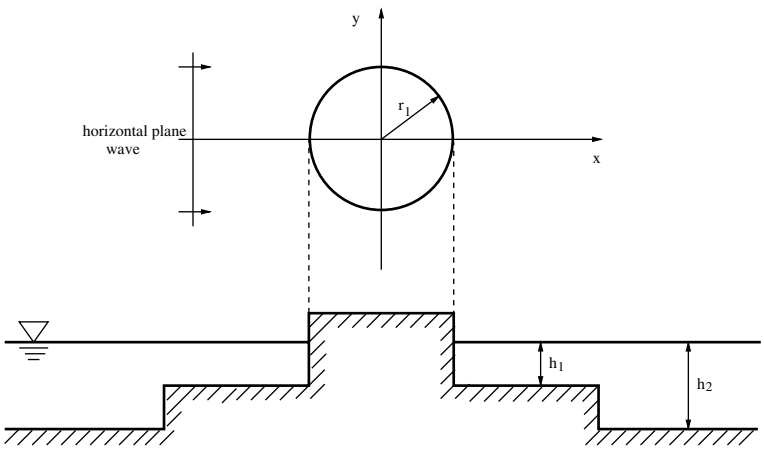

Fig. 7. Plane wave scattered by a rigid cylinder.

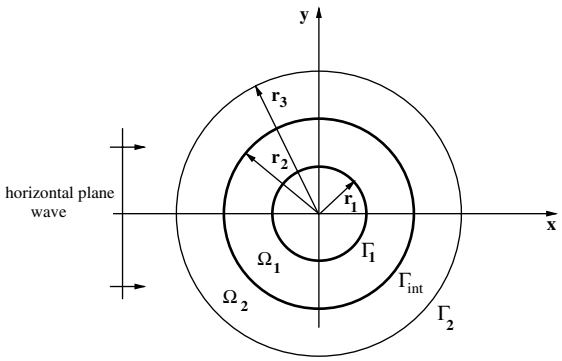

Fig. 8. Plane wave scattered by a rigid cylinder.

$$\Phi_1 = \sum_{n=0}^{\infty} [A_n J_n(k_1 r) + B_n Y_n(k_1 r)] \cos n\theta \tag{23}$$

and

$$\Phi_2 = \sum_{n=0}^{\infty} [C_n J_n(k_2 r) + D_n Y_n(k_2 r)] \cos n\theta, \tag{24}$$

where J_n and Y_n are first and second kind Bessel functions of order n. The coefficients A_n, B_n, C_n and D_n are determined by the following boundary conditions

- Neumann boundary condition on the scatterer

$$\frac{\partial \Phi_1}{\partial r} = 0 \quad \text{at } r = r_1. \tag{25}$$

- Continuity of potential at the interface Γ_{int}

$$\Phi_1 = \Phi_2 \quad \text{at } r = r_2. \tag{26}$$

- Flux equilibrium at the interface Γ_{int}

$$\frac{1}{k_1^2}\frac{\partial \Phi_1}{\partial r} = \frac{1}{k_2^2}\frac{\partial \Phi_2}{\partial r} \quad \text{at } r = r_2 \tag{27}$$

- at the exterior boundary Γ_2, the scattered potential behaves as $\exp(\mathrm{i}k_2 r)/\sqrt{r}$, this is true only if the boundary Γ_2 is far enough from the scatterer. Therefore, a simple form of absorbing condition is given

$$\frac{\partial \Phi_S}{\partial r} + \frac{\Phi_S}{2r} - \mathrm{i}k_2 \Phi_S = 0 \quad \text{at } r = r_3. \tag{28}$$

Since $\Phi_2 = \Phi_S + \Phi_I$, where Φ_I is the potential of the incident plane wave, we can write

$$\frac{\partial \Phi_2}{\partial r} + \left(\frac{1}{2r} - \mathrm{i}k_2\right)\Phi_2 = \frac{\partial \Phi_I}{\partial r} + \left(\frac{1}{2r} - \mathrm{i}k_2\right)\Phi_I, \tag{29}$$

where the potential Φ_I can be expanded into a combination of Bessel functions of the first kind as follows

$$\Phi_I = \sum_{n=0}^{\infty} \mathrm{i}^n \varepsilon_n J_n(k_2 r) \cos n\theta \tag{30}$$

with $\varepsilon_0 = 1$ and $\varepsilon_n = 2$ for $n = 1, 2, 3, \ldots$.

Once the coefficients A_n, B_n, C_n and D_n are obtained up to a truncation order, the analytical expressions for Φ_1 and Φ_2 can be evaluated at any point of the subdomains Ω_1 and Ω_2, respectively.

7.2. Numerical solution

The scattering problem to solve is expressed by the general system (21) where the bloc matrices are given by

$$H_1 = \int_{\Omega_1} (\nabla \boldsymbol{P}_1^{\mathrm{T}} \nabla \boldsymbol{P}_1 - k_1^2 \boldsymbol{P}_1^{\mathrm{T}} \boldsymbol{P}_1)\, \mathrm{d}\Omega, \tag{31}$$

$$H_2 = \int_{\Omega_2} (\nabla \boldsymbol{P}_2^{\mathrm{T}} \nabla \boldsymbol{P}_2 - k_2^2 \boldsymbol{P}_2^{\mathrm{T}} \boldsymbol{P}_2)\, \mathrm{d}\Omega + \int_{\Gamma_2} \boldsymbol{P}_2^{\mathrm{T}} \left(\frac{1}{2r} - \mathrm{i}k_2\right) \boldsymbol{P}_2\, \mathrm{d}\Gamma, \tag{32}$$

$$C_1 = k_1^2 \int_{\Gamma_{\mathrm{int}}} \boldsymbol{P}_1^{\mathrm{T}} \boldsymbol{Q}\, \mathrm{d}\Gamma, \tag{33}$$

$$C_2 = k_2^2 \int_{\Gamma_{\mathrm{int}}} \boldsymbol{P}_2^{\mathrm{T}} \boldsymbol{Q}\, \mathrm{d}\Gamma, \tag{34}$$

$$\boldsymbol{f}_1 = 0, \tag{35}$$

and

$$\boldsymbol{f}_2 = \int_{\Gamma_2} \boldsymbol{P}_2^{\mathrm{T}} \left[\frac{1}{2r} + (\cos\theta - 1)\mathrm{i}k_2\right] \mathrm{e}^{\mathrm{i}k_2 r \cos\theta}\, \mathrm{d}\Gamma. \tag{36}$$

The computational domain around the cylinder is meshed into 4-noded finite elements with exactly mapped geometry. We define the number of degrees of freedom per wavelength τ by

$$\tau = \sqrt{\frac{N}{\frac{S_1}{\lambda_1^2} + \frac{S_2}{\lambda_2^2}}} \tag{37}$$

where N is the total number of variables needed to represent the potentials in both regions Ω_1 of surface S_1 and Ω_2 of surface S_2, with wavelengths λ_1 and λ_2, respectively. For a radial mesh with I nodes in the radial direction and J nodes in the angular direction, then the total number of degrees of freedom is given by $N = (I + 2) \times J \times M$, where M is the number of plane waves attached to each node. Note that the $(I + 2)$ term comes from the fact that the nodes at the interface Γ_{int} must be duplicated and Lagrange multiplier edge elements introduced (Fig. 3). In this study, the number M of plane waves attached at each node is chosen to be constant.

The accuracy of the model is measured by the relative $L_2(\Omega)$-norm error defined, in the whole computational domain $\Omega = \Omega_1 \cup \Omega_2$, by

$$\varepsilon_2 = \frac{\|\Phi_{\mathrm{ana}} - \Phi_{\mathrm{num}}\|_{L^2(\Omega)}}{\|\Phi_{\mathrm{ana}}\|_{L^2(\Omega)}}, \tag{38}$$

where Φ_{ana} and Φ_{num} are the analytical and numerical solution of the total potential around the cylinder, respectively.

7.3. Numerical results and discussion

The mesh of the computational domain around the cylinder (Fig. 9) contains 54 nodes and 36 elements. The radius of the cylinder is equal to a unit of length. The interface between Ω_1 and Ω_2 is at $r_2/r_1 = 2$ and the outer boundary Γ_2 is situated at $r_3/r_1 = 3$. The horizontal plane wave of a unit amplitude is incident from the negative x-axis, in the outer region with the wavenumber k_2. It is transmitted to the inner region with the wavenumber k_1, hits the cylinder then radiates towards infinity by passing again through the interface Γ_{int}. Figs. 10–12 show the total potential around the diffracting cylinder for the cases $(k_1, k_2) = (\pi, 5\pi)$, $(10\pi, 6\pi)$ and $(10\pi, 2\pi)$. The numerical results are reported on the meshed half surface around the cylinder and the analytical results are reported on the other half. For the first case, $(k_1, k_2) = (\pi, 5\pi)$, The region around the cylinder is deeper than the outer one ($h_1 > h_2$). The wavelength λ_2, in the outer domain Ω_2, is shorter than λ_1 and the ratio $\lambda_1/\lambda_2 = 5$. Fig. 10 shows that the incident wave is mainly reflected at the

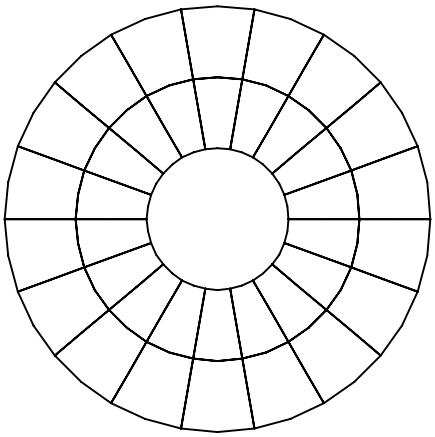

Fig. 9. Mesh of the computational domain.

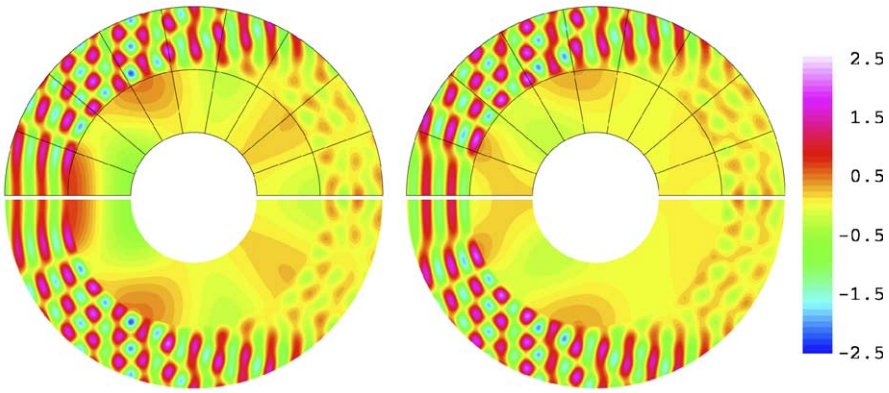

Fig. 10. Total potential around the cylinder, $k_1 = \pi$, $k_2 = 5\pi$, $\tau = 5.6$, $\varepsilon_2 = 1.6\%$, (left) real part, (right) imaginary part.

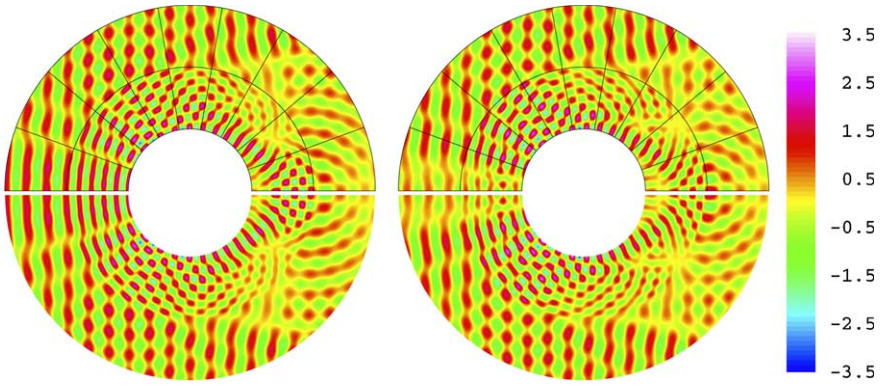

Fig. 11. Total potential around the cylinder, $k_1 = 10\pi$, $k_2 = 6\pi$, $\tau = 3.4$, $\varepsilon_2 = 0.4\%$, (left) real part, (right) imaginary part.

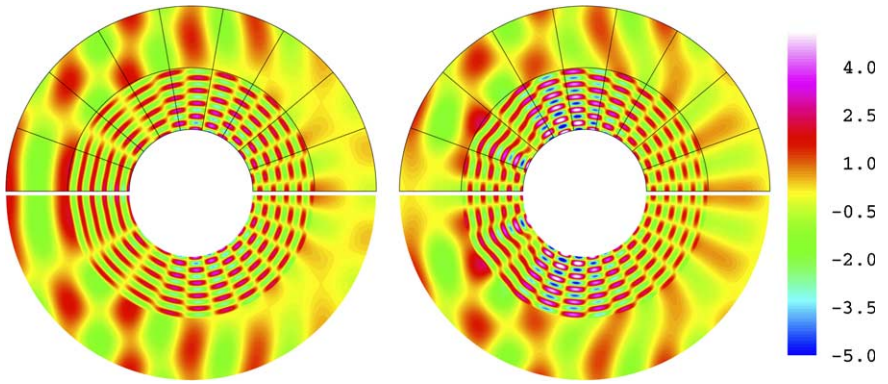

Fig. 12. Total potential around the cylinder, $k_1 = 10\pi$, $k_2 = 2\pi$, $\tau = 4.2$, $\varepsilon_2 = 0.07\%$, (left) real part, (right) imaginary part.

Table 1
Plane wave scattering by a rigid circular cylinder, $k_1 = 2k_2$

k_1	2π	4π	6π	8π	10π	12π	14π	16π	18π	20π
τ	25.9	12.9	8.6	6.5	5.2	4.3	3.7	3.2	2.8	2.6
ε_2 [%]	0.002	0.007	0.02	0.1	0.5	2.5	0.9	0.4	0.6	1.1

interface boundary Γ_{int} and most of the interferences occur in the outer region. The inner region and the shadow zone of the outer region look calm. For this case, 36 plane waves are attached at each node, which gives $\tau = 5.6$. The L_2 error is 1.6% but the discrepancies are too small to be seen. For examples where $(k_1, k_2) = (10\pi, 6\pi)$ and $(10\pi, 2\pi)$, in both cases, 50 plane waves evenly spaced are attached at each node. This lead to 3.4 degrees of freedom per wavelength (DOF/λ) in the first example and 4.2 DOF/λ in the second example. The L_2 error is 0.4% and 0.07%, respectively. This shows a drastic reduction in the total number of degrees of freedom needed to solve such problems. On the figures, it is obvious that the wavelengths are different between the two regions Ω_1 and Ω_2. In Fig. 11, the ratio $\lambda_1/\lambda_2 = 0.6$ and therefore the transition at the interface Γ_{int} is quite smooth. However, in Fig. 12, the ratio $\lambda_1/\lambda_2 = 0.2$ and the shorter waves in the inner region Ω_1 appear to be imprisoned between the rigid cylinder and the region Ω_2 of longer waves and the potential in the domain Ω_1 presents high amplitudes.

In the following study, for the same mesh of Fig. 9, a constant number $N = 100$ of plane waves are attached at each node. The wavenumber k_1 varies from 2π to 20π and k_2 is taken such that $k_1 = 2k_2$. The performance of the method are reported in Table 1 for different values of k_1. The table gives the number of degrees of freedom per wavelength τ and the corresponding L_2 error for each test case. For low wavenumbers, the parameter τ is bigger than the usual number of 'ten nodal points per wavelength' used as a 'rule of thumb' requirement for the conventional polynomial finite elements wave problems. However, the error is much smaller. For the higher wavenumbers ($k_1 \geqslant 14\pi$), τ falls to around 3 and the L_2 error stays within engineering accuracy limit.

8. Conclusions

This paper has demonstrated that the interface conditions between zones of different waves speeds can be applied effectively using a Lagrange multiplier approach. The formulation is straightforward and

uncomplicated. The program has solved problems for which analytical solutions exist in which waves pass from a zone of one wave speed to a zone with a different wave speed. All the expected interface effects are recovered, including Snell's law and the generation, when appropriate, of evanescent, or edge waves. The accurate prediction of the edge waves is especially gratifying since they are not explicitly present in the solution space. The program has also solved a range of circular problems with regions of different wave speeds and again excellent agreement with the analytical solutions has been obtained.

It should also be possible to extend the method to three dimensions, since wave propagation in three dimensions, while more complicated, does not present any new features beyond the two dimensional case.

Acknowledgment

Omar Laghrouche is grateful to the EPSRC for funding this work under EPSRC grant number GR/M41025. Emmanuel Perrey-Debain is grateful to the EPSRC for funding this work under EPSRC grant number GR/N09879. Peter Bettess is grateful to the EPSRC Senior Research Fellowship committee, chaired by Professor Richard Brook, which is funding related wave modelling work through EPSRC Grant Number SF/000169.

References

[1] F. Ihlenburg, I. Babuška, Dispersion analysis and error estimation of Galerkin finite element methods for the Helmholtz equation, Int. J. Numer. Methods Engrg. 38 (1995) 3745–3774.
[2] I. Babuška, F. Ihlenburg, T. Strouboulis, S. Gangaraj, A posteriori error estimation for finite element solutions of Helmholtz' equation. Part I. The quality of local indicators and estimators, Int. J. Numer. Methods Engrg. 40 (1997) 3443–3462.
[3] I. Babuška, F. Ihlenburg, T. Strouboulis, S. Gangaraj, A posteriori error estimation for finite element solutions of Helmholtz' equation. Part II. Estimation of pollution error, Int. J. Numer. Methods Engrg. 40 (1997) 3883–3900.
[4] M. Ainsworth, Discrete dispersion relation for hp-finite element approximation at high wave number, Preprint NI03005-CPD, Newton Institute for Mathematical Sciences, Cambridge 2003.
[5] Proceedings of London Mathematical Society, LMS Durham Symposium: Computational Methods for the Wave Propagation in Direct Scattering, 2002.
[6] P. Bettess, O. Laghrouche, E. Perrey-Debain (Eds.), Theme issue on short wave scattering, Philos. Trans. R. Soc. Lond. A 362 (2004).
[7] J.M. Melenk, I. Babuška, The partition of unity finite element method. Basic theory and applications, Comput. Methods Appl. Mech. Engrg. 139 (1996) 289–314.
[8] I. Babuška, J.M. Melenk, The partition of unity method, Int. J. Numer. Methods Engrg. 40 (1997) 727–758.
[9] O. Laghrouche, P. Bettess, Short wave modelling using special finite elements, J. Comput. Acoust. 8 (2000) 189–210.
[10] O. Laghrouche, P. Bettess, R.J. Astley, Modelling of short wave diffraction problems using approximating systems of plane waves, Int. J. Numer. Methods Engrg. 54 (2002) 1501–1533.
[11] P. Ortiz, E. Sanchez, An improved partition of unity finite element model for diffraction problems, Int. J. Numer. Methods Engrg. 50 (2001) 2727–2740.
[12] E. Perrey-Debain, J. Trevelyan, P. Bettess, New special boundary elements for short wave problems, Commun. Numer. Methods Engrg. 18 (2002) 259–268.
[13] E. Perrey-Debain, J. Trevelyan, P. Bettess, Plane wave interpolation in direct collocation boundary element method for radiation and wave scattering: numerical aspects and applications, J. Sound Vib. 261 (2003) 839–858.
[14] C. Farhat, I. Harari, L. Franca, The discontinuous enrichment method, Comput. Methods Appl. Mech. Engrg. 190 (2001) 6455–6479.
[15] C. Farhat, I. Harari, U. Hetmanuk, A discontinuous Galerkin method with Lagrange multipliers for the solution of Helmholtz problems in the mid-frequency regime, Comput. Methods Appl. Mech. Engrg. 192 (2003) 1389–1419.
[16] O. Laghrouche, P. Bettess, E. Perrey-Debain, J. Trevelyan, Plane wave basis for wave scattering in three dimensions, Commun. Numer. Methods Engrg. 19 (2003) 715–723.
[17] E. Perrey-Debain, O. Laghrouche, P. Bettess, J. Trevelyan, Plane wave basis finite lements and boundary elements for three dimensional wave scattering, Philos. Trans. R. Soc. Lond. A 362 (2004) 561–577.

[18] R.J. Astley and P. Gamallo, Special short wave elements for flow acoustics, Comput. Methods Appl. Mech. Engrg., in this issue.
[19] O. Cessenat, B. Després, Application of an ultra weak variational formulation of elliptic PDEs to the two dimensional Helmholtz problem, SIAM J. Numer. Anal. 35 (1998) 255–299.
[20] T. Huttunen, P. Monk, J.P. Kaipio, Computation aspects of the ultra weak variational formulation, J. Comput. Phys. 182 (2002) 27–46.
[21] T. Huttunen, P. Monk, F. Collino, J.P. Kaipio, The ultra weak variational formulation for elastic wave problems, J. Comput. Phys., in press).
[22] P. Bettess, Special wave basis finite elements for very short wave refraction and scattering problems, Commun. Numer. Methods Engrg. 20 (2004) 291–298.
[23] P. Ortiz, Finite elements using plane wave basis for scattering of surface water waves, Philos. Trans. R. Soc. Lond. A 362 (2004) 525–540.
[24] R. Sugimoto, P. Bettess, J. Trevelyan, A numerical integration scheme for special quadrilateral finite elements for Helmholtz equation, Commun. Numer. Methods Engrg. 19 (2002) 233–245.
[25] P. Bettess, J. Shirron, O. Laghrouche, B. Peseux, R. Sugimoto, J. Trevelyan, A numerical integration scheme for special finite elements for Helmholtz equation, Int. J. Numer. Methods Engrg. 56 (2003) 531–552.